

# RSC Advances



This is an *Accepted Manuscript*, which has been through the Royal Society of Chemistry peer review process and has been accepted for publication.

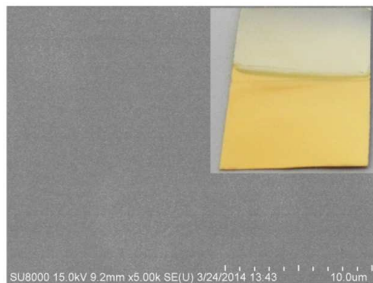
*Accepted Manuscripts* are published online shortly after acceptance, before technical editing, formatting and proof reading. Using this free service, authors can make their results available to the community, in citable form, before we publish the edited article. This *Accepted Manuscript* will be replaced by the edited, formatted and paginated article as soon as this is available.

You can find more information about *Accepted Manuscripts* in the [Information for Authors](#).

Please note that technical editing may introduce minor changes to the text and/or graphics, which may alter content. The journal's standard [Terms & Conditions](#) and the [Ethical guidelines](#) still apply. In no event shall the Royal Society of Chemistry be held responsible for any errors or omissions in this *Accepted Manuscript* or any consequences arising from the use of any information it contains.

## TOC

Golden bright gold electrodeposit with smooth and compact surface could be obtained from the introduced cyanide-free gold electroplating electrolyte.



# **Experimental and Theoretical Studies of DMH as Complexing Agent for Cyanide-free Gold Electroplating Electrolyte**

Xuefeng Ren, Ying Song, Anmin Liu, Jie Zhang, Peixia Yang, Jinqiu Zhang, and  
Maozhong An\*

*State Key Laboratory of Urban Water Resource and Environment, School of Chemical Engineering and Technology, Harbin Institute of Technology, Harbin, 150001, China.*

**Abstract:** In this paper, a cyanide-free gold electroplating electrolyte using 5,5-dimethylhydantoin(DMH) as complexing agent was introduced. Golden bright gold electrodeposit with smooth and compact surface was obtained from the introduced cyanide-free gold electroplating electrolyte. The results of scanning electron microscope (SEM) measurements confirmed that the golden bright gold electrodeposit possess an excellent leveling capability as well as smooth and compact morphology. The crystalline structure of the gold electrodeposits was characterized by X-ray diffraction (XRD) analysis. Computational chemistry was employed to get an insight view of the reason for selecting DMH from hydantoin derivatives as the complexing agent for the introduced cyanide-free gold electroplating electrolyte. Quantum chemical calculations were employed to study the electronic properties and orbital information of the investigated complexing agents. The adsorption interactions between these complexing agents and the metal surfaces were investigated by molecular dynamic (MD) simulations. Consequently, the results of these theoretical studies revealed that due to its strong electron donating abilities and high adsorption energies on metal surfaces, DMH was selected from hydantoin derivatives as the complexing agent of the introduced cyanide-free gold electroplating electrolyte.

## 1. Introduction

Owing to their excellent physical, chemical, and conductive properties, gold electrodeposits obtained from cyanide-based gold electroplating electrolytes have been widely used in jewelries, artware, electronics, and aerospace industries for more than 100 years.<sup>1-4</sup> Unfortunately, as one of the most toxic chemicals, cyanide brings extremely high risks to human health and the environment.<sup>5-7</sup> Numerous cyanide-free gold electroplating electrolytes have been developed to replace the cyanide-based electrolytes for gold electroplating.<sup>8-12</sup> However, except for few successful cases, most of them were unsatisfying for the poor-quality of electroplating electrolytes or gold electrodeposits.<sup>13</sup> More works on the investigation of complexing agents are needed for the development of cyanide-free gold electroplating electrolyte.

Hydantoin is a low cost and commercially available heterocyclic organic with good solubility and stability in aqueous solutions in a large temperature range.<sup>14</sup> Its derivatives are promising and stable complexing agents for several metal ions.<sup>15, 16</sup> Among a series of hydantoin derivatives, 5,5-dimethylhydantoin (DMH) was selected as complexing agent for cyanide-free gold electroplating electrolyte in our study. A golden bright gold electrodeposit was obtained with the addition of some additives in the investigated cyanide-free gold electroplating electrolyte. Besides the application of DMH in the introduced cyanide-free gold electroplating electrolyte, DMH was employed as complexing agents for silver and copper electroplating in our previous studies.<sup>17-20</sup> It is of important significance to get an insight view of the reasons to select DMH from hydantoin derivatives as the complexing agents for the introduced cyanide-free gold electroplating electrolyte and other metal electroplating electrolytes.

Studying the mechanism of complexing agents for cyanide-free gold electroplating electrolytes through experimentation is extravagant both in time and

resources, especially for the consumption of the extremely precious gold. Time-saving techniques, such as quantum chemical calculations<sup>21-24</sup> and molecular dynamic (MD) simulations<sup>25</sup>, are useful and urgently needed methods to study the organometallic compound or select complexing agents for cyanide-free metal electroplating electrolyte. To investigate their behaviors in small chemical systems at the molecular level, quantum chemical calculations and MD simulations are emerging areas of all these researches for chemistry.<sup>26-34</sup> In the coordinate systems, bonding interactions between metal ions and complexing agents can be predicted and investigated by quantum chemical calculations.<sup>35-38</sup> Quantum chemical calculations and MD simulations are convenient methods to study the properties of complexing agents<sup>39-41</sup>, additives<sup>42, 43</sup>, inhibitors<sup>44-51</sup>, and other molecules<sup>52-58</sup> as well as their adsorption behaviors on metal surfaces.

In this work, the electronic properties and orbital information of hydantoin and its derivatives were demonstrated by quantum chemical calculations. MD simulations were employed to reveal the adsorption interactions between all these studied organics and the metal surfaces. The results of these theoretical studies revealed that due to its strong electron donating abilities and high adsorption energies on metal surfaces, DMH could be the optimal choice selected from hydantoin derivatives as the complexing agent of the introduced cyanide-free gold electroplating electrolyte.

## 2. Experimental

### 2.1. Measurements and Apparatus

The gold electroplating electrolyte was prepared with 0.025 mol/L  $\text{HAuCl}_4$ , 0.3 mol/L DMH, 0.36 mol/L  $\text{K}_2\text{CO}_3$ , and 30 mg/L PEI in deionized water. All the

reagents used in this work were analytical grade. The pH of all the electrolytes was maintained at 10. Gold electrodeposits used for performance measurements were prepared under galvanostatic condition ( $8 \text{ mA/cm}^2$ ) with mild agitation at 318 K in a cell employing an insoluble anode and a copper substrate with nickel electrodeposit coated. Field emission scanning electron microscopy (FE-SEM, Hitachi SU8000) was used to study the surface morphologies and composition of the gold electrodeposits. The crystalline structure of the gold electrodeposits was characterized by XRD analysis with a D/max-3C x-ray diffractometer at a scanning rate of  $0.02^\circ/\text{s}$  with  $\text{Cu K}\alpha$  radiation.

## 2.2. Quantum chemical calculations and MD simulations

All quantum chemical calculations were carried out by density functional theory (DFT) methods using B3LYP exchange-correlation functional method. In all these quantum chemical calculations, 6-311G\*\* basis set was used for hydrogen, carbon, nitrogen, oxygen, chlorine, and bromine atoms of the studied systems, respectively. All calculations on these systems under investigation were performed using Gaussian 09 program package at 298 K with water as solvent in the IEFPCM theoretical model.

Simulations of the adsorption interactions between the studied organics and the nickel and gold surfaces were carried out in a simulation box with periodic boundary conditions using Materials Studio (from Accelrys Inc.). The box consisted of a nickel or gold surface (cleaved along the (111) plane, with volume  $2.88 \text{ nm} \times 2.88 \text{ nm} \times 1.18 \text{ nm}$  of Au and  $2.49 \text{ nm} \times 2.49 \text{ nm} \times 1.02 \text{ nm}$  of Ni, respectively.), a liquid phase, and a vacuum layer of 1 nm height. The liquid phase was water molecules with a density of  $1 \text{ g/cm}^3$  and containing 3 studied organics. The MD simulations were performed at 298 K, utilizing an NVT ensemble and the ab initio polymer consistent force field (PCFF), with a time step of 1 fs and simulation time of 500 ps.

The interaction energy between the metal surface and organic molecules was calculated using equation (1).

$$E_{Interaction} = E_{Total} - E_{Metal} - E_{Agents} \quad (1)$$

$E_{Total}$  was the total energy of the gold or nickel crystal together with the adsorbed organics.  $E_{Metal}$  and  $E_{Agents}$  were the total energy of the gold or nickel crystal and free agents, respectively.

### 3. Results and discussion

#### 3.1 Function of DMH in the gold electroplating

With DMH as the complexing agent, golden bright gold electrodeposit was obtained from the introduced gold electroplating electrolyte in the presence of suitable additive. Fig. 1 displays the macroscopic images of gold electrodeposits obtained from the introduced cyanide-free gold electroplating electrolyte with and without additive, as well as the  $\text{HAuCl}_4$  electrolyte without DMH.

It can be seen clearly that gold electrodeposit in Fig. 1 (a) is golden bright with smooth and compact surface. This indicates that the introduced cyanide-free electrolyte is effective to produce excellent gold electrodeposit, which meets the request of application in decorative purposes. As displayed in Fig. 1 (b) and (c), the appearances of the gold electrodeposits obtained from the electrolyte without additive and the  $\text{HAuCl}_4$  electrolyte without DMH were all brown. However, the gold electrodeposits obtained from the electrolyte with DMH and without additive had a relatively more uniform surface.

The surface morphology of the gold electrodeposits obtained from the introduced cyanide-free gold electroplating electrolyte with and without additive, as well as the  $\text{HAuCl}_4$  electrolyte without DMH was characterized by SEM measurements. SEM top

view images of the gold electrodeposits obtained from the introduced cyanide-free gold electroplating electrolyte with and without additive, as well as the  $\text{HAuCl}_4$  electrolyte without DMH were displayed in Fig. 2.

It can be seen from Fig. 2 (e) and (f) that the gold electrodeposits obtained from the  $\text{HAuCl}_4$  electrolyte without DMH possess rough and loosened morphologies with big crystal grains. Fig. 2 (c) and (d) showed that the crystal grains of gold electrodeposit obtained from DMH based gold electroplating electrolyte without additive were smaller than that from the  $\text{HAuCl}_4$  electrolyte without DMH and the surface was more smooth and compact. These observations most likely originated from using DMH as complexing agent, which caused an increase of the cathodic polarization and resulted in smaller grains in the gold electrodeposit. As displayed in Fig. S1 (Supplementary Information), after immersed the copper substrate with nickel electrodeposit coated into the introduced cyanide-free gold electroplating electrolyte with additive and without additive, no difference was observed on the surface after the immersion. Thus, as DMH employed as complexing agent in the electrolyte to coordinate with  $\text{HAuCl}_4$  to form  $[\text{Au}(\text{DMH})_4]^-$ , the stability of  $\text{HAuCl}_4$  was significantly improved and no strike-plating process was necessary to obtain good adherent gold deposits on the substrate using the introduced gold plating electrolyte containing DMH as complexing agent.

However, the gold electrodeposit obtained from the cyanide-free gold electroplating electrolyte with additive is more smooth and compact with smaller crystal grains than that from electrolyte without additive, as shown in Fig. 2 (a) and (b). These results provide an indication that the surface quality of the gold electrodeposit could be further improved by the addition of suitable additive. In order to distinguish the role of DMH and additive in the gold electroplating electrolyte, the

additive was added into the  $\text{HAuCl}_4$  electrolyte without DMH to gain gold electrodeposit from  $\text{HAuCl}_4$  electrolyte without DMH but with additive. Unfortunately, when the additive was added into the  $\text{HAuCl}_4$  electrolyte without DMH, the  $\text{HAuCl}_4$  electrolyte become turbid and precipitation was formed, as displayed in Fig. S2 (d) (Supplementary Information). However, Fig. S2 (c) showed that no changes to the electrolyte were detected after it was used for many times gold electroplating, indicating that the gold electroplating electrolyte possesses good stability. DMH was employed as complexing agent in the introduced electrolyte to coordinate with  $\text{HAuCl}_4$  to form  $[\text{Au}(\text{DMH})_4]^+$ , and the stability of  $\text{HAuCl}_4$  was significantly improved. And the influence of additive on the electrochemical behavior and gold deposit of the introduced cyanide-free electrolyte were investigated using electrochemical measurements and materials characterizations.<sup>59</sup>

The phase structures of the gold electrodeposits obtained from the introduced cyanide-free gold electroplating electrolyte with and without additive, as well as the  $\text{HAuCl}_4$  electrolyte without DMH were confirmed by EDS and XRD. All these electrodeposits obtained from the introduced cyanide-free gold electroplating electrolyte with and without additive, as well as the  $\text{HAuCl}_4$  electrolyte without DMH were pure gold and the purity of the gold deposit was very high as showed in the EDS patterns (Fig. S3 in Supplementary Information). XRD patterns of the gold electrodeposits obtained from the introduced cyanide-free gold electroplating electrolyte with and without additive, as well as the  $\text{HAuCl}_4$  electrolyte without DMH were displayed in Fig. 3.

As displayed in Fig. 3, all peaks can be indexed to Au (111), (200), (220), (311), (222) and (400) crystal face without any additional peak observed when the gold electrodeposits obtained from the introduced cyanide-free gold electroplating

electrolyte with additive and without additive. However, a peak corresponding to Cu (220) was detected on the pattern of gold electrodeposits obtained from  $\text{HAuCl}_4$  electrolyte without DMH. It indicates that the Cu substrate was partially exposed after the gold electroplating in the  $\text{HAuCl}_4$  electrolyte without DMH, which can be confirmed by the replacement reaction of a copper substrate with nickel electrodeposit coated in the  $\text{HAuCl}_4$  electrolyte without DMH as shown in Fig. S1. As the surface morphology of the gold electrodeposits displayed in Fig. 2 (e) and (f), the gold electrodeposits obtained from the  $\text{HAuCl}_4$  electrolyte without DMH possess rough and loosened morphologies with big crystal grains. The rough and loosened gold electrodeposits make the expose of copper substrate possible.

### 3.2 Quantum chemical calculations

The molecular structures of hydantoin and its usual derivatives molecules, including aminohydantoin (AHD), 1-bromo-3-chloro-5,5-dimethylhydantoin (BCDMH), 1,3-dibromo-5,5-dimethylhydantoin (DBDMH), 1,3-dichloro-5,5-dimethylhydantoin (DCDMH), dimethyloldimethyl hydantoin (DMDMH), 5,5-dimethylhydantoin (DMH), and 1,5,5-trimethylhydantoin (TMH), are shown in Fig. S4 (Supplementary Information). It is of important significance to get an insight view of the reasons for selecting DMH from hydantoin derivatives as the complexing agent for the introduced cyanide-free gold electroplating electrolyte.

As displayed in Fig. S4, all these studied organics have the same nitrogen containing five-membered ring with the same C=O bond and different substituents, which might generate diversiform influences on the electronic properties and frontier molecular orbital information of all these studied organics. It indicated that these organic molecules showed different ability to form gold-complex coordinated bonds and adsorb on the metal surfaces due to their probable different electronic properties

and frontier molecular orbital information. Quantum chemical calculations were conducted to reveal the electronic properties and frontier molecular orbital information of all these studied organics to verify the prediction.

Fig. S5 (Supplementary Information) exhibits the distribution of the HOMO and electron cloud densities of the studied hydantoin and its usual derivatives. The distribution of LUMO is displayed in Fig. S6 (Supplementary Information).

The presence of nitrogen and oxygen atoms showed significant contributions to the HOMO as displayed in Fig. S5. This was due to the electron donating properties of the nitrogen and oxygen atoms, resulting in the ability to form gold-complex coordinated bonds. With the replacement of hydrogen atoms by chlorine atoms, bromine atoms or methylol, BCDMH, DBDMH, DCDMH, and DMDMH manifested more complicated localization of HOMO than DMH, as displayed in Fig. S5 (b) ~ (d), (e) and (f).

Molecules (b)~(d) in Fig. S6 show a similar localization of the LUMO and high electron cloud densities, indicating similar electronic properties and strong electron accepting abilities. On the other hand, molecules (a) possessed the similar electronic properties and electron accepting abilities with molecules (e)~(h).

In addition to the localization of the molecular orbitals,  $E_{\text{HOMO}}$ ,  $E_{\text{LUMO}}$ , and their difference ( $\Delta E$ ) are useful tools to characterize the electronic properties and adsorption behaviors of each molecule. According to the frontier molecular orbital theory, the energy of the highest occupied molecular orbital (HOMO) and lowest unoccupied molecular orbital (LUMO) are often associated with the electron donating ability and electron accepting ability of organic molecules. Higher values of  $E_{\text{HOMO}}$  (energy of HOMO) and lower values of  $E_{\text{LUMO}}$  (energy of LUMO) indicate a tendency of a molecule to donate and accept electrons, respectively.  $E_{\text{HOMO}}$  and  $E_{\text{LUMO}}$ , along

with  $\Delta E$  are important molecular electronic properties that relate to the behavior and adsorption properties of studied organics. A schematic depiction of these values based on frontier molecular orbitals is presented in Fig. 4.

As displayed in Fig. 4, structures (d), (e), (f), and (g) have similarly, relatively high  $E_{\text{HOMO}}$  values of -7.393 eV, -7.343 eV, -7.404 eV, and -7.444 eV, respectively. They are likely good complexing agents owing to their propensity to donate electrons to gold ions and form coordinated gold-complex structures. The difference between the frontier molecular orbitals of these structures was mainly in the  $E_{\text{LUMO}}$ . With relatively high  $E_{\text{LUMO}}$  values of -0.427 eV of structure (f) and -0.392 eV of structure (h), respectively, indicating that these two organics have a similar weak ability to form back-donation bonds when accepting electrons from the anti-bonding orbitals within gold ions. On the other hand, the higher  $E_{\text{LUMO}}$  values of DMH imply that acceptance of electrons from the gold ions and cathodic metal atoms are more difficult relative to other structures by forming an anti-bond with the cathodic metals and ions. Thus, the coordinated gold-complex of DMH and gold ions may be the most stable in all the coordinated gold-complex of all these studied organics and gold ions.

$\Delta E$  values lead to different stabilities of the adsorption layers formed by complexing agent on the metal surface.<sup>60, 61</sup> The smallest  $\Delta E$  calculated from structures (d)~(g) suggests that DCDMH has a more effective adsorption on the metal surfaces. On the other side, the higher  $E_{\text{LUMO}}$  value of structure (d) implies that acceptance of electrons from the cathodic metal atoms or ions are easier to forming anti-bond with the cathodic metals or ions. Thus, the stability of coordinated gold-complex or the adsorption of structure (d) on the metal surface may be decreased.

To investigate the ability to form the gold-complexes coordinate bonds, quantum

chemical calculations were employed to study the charge distributions of all these studied complexing agents. The charge distributions of the studied organic molecules are shown in Fig. 5.

As the charge distributions shown in Fig. 5, with low electronegativity to be an electron donor, nitrogen and oxygen atoms in all these studied organics as well as the chlorine and bromine atoms in structures (b)~(d) might be the possible atoms forming coordinate bonds with gold ions. Combined the frontier molecular orbital information and the charge distributions showed in Fig. 5, structures (e), (f), and (g) are likely better complexing agents owing to their propensity to donate electrons to gold ions and form gold-complex coordinated bonds.

### 3.3 MD simulations

The adsorption behaviors of all the studied complexing agents on Ni (111) and Au (111) surfaces were performed by MD simulations in this work. Results of AHD simulations are shown in the manuscript and the remainders in the Supplementary Information due to space limitations. The adsorption behaviors of AHD on Au (111) and Ni (111) surfaces are shown in Fig. 6 and Fig. S7, respectively. Fig. 6 (a) reveals the initial configuration of the MD simulation boxes. Fig. 6 (b) displays the final equilibrium configuration of the MD simulation boxes at 298 K with a time step of 1 fs and simulation time of 500 ps. Fig. 6 (c) shows the top view of the final equilibrium configuration of the simulation boxes. Fig. 6 (d) and 6 (e) shows the energy and temperature fluctuation curves of the MD simulations. These plots indicate that the systems were already at equilibrium with the completion of the simulation.

The adsorption energies and MD simulation boxes of all the other studied complexing agents are summarized in Table 1 and Fig. S7 ~ Fig. S21 (Supplementary

Information), respectively.

The main conclusions drawn from these simulations illustrate that all these studied complexing agents could adsorb on the metal surfaces with high energies. Moreover, as shown in the (c) of Fig. 6 and Fig. S7 ~ Fig. S21 (Supplementary Information), heterocyclic rings of these studied organics were virtually parallel to the nickel and gold surfaces, suggesting effective adsorption on the metal surfaces. Results of MD simulations manifested that all the investigated hydantoin derivatives could adsorb on the nickel and gold surfaces strongly, leading to a higher inhibited effect for gold electrodeposition on the nickel and gold surfaces.

Summarily, on the results of DFT calculations and MD simulations, with a relatively high  $E_{\text{HOMO}}$  value and effective adsorptions on the nickel, gold, silver, copper, and iron surfaces, DMH, with environmental compatibility, low cost, good solubility, and superior stability in alkaline solution within a large temperature range, could be the optimal choice from hydantoin derivatives as the complexing agent for cyanide-free gold electroplating electrolyte and other metal electroplating electrolytes due to its strong electron donating abilities and high adsorption energies on metal surfaces.

#### 4. Conclusions

In conclusion, we report a cyanide-free gold electroplating electrolyte using 5,5-dimethylhydantoin(DMH) as complexing agent. The cyanide-free electrolyte is stable and environmental friendly with low toxicity. With the addition of suitable additive into the investigated cyanide-free gold electroplating electrolyte, golden bright gold electrodeposit with smooth and compact surface was obtained. SEM images confirm that the gold electrodeposit has excellent leveling capability as well as smooth and compact morphology. This indicates the introduced gold electroplating

electrolyte is a promising candidate to replace the conventional cyanide-based gold electroplating electrolyte. Computational chemistry was employed to get an insight view of the reasons for selecting DMH from hydantoin derivatives as the complexing agent for the introduced cyanide-free gold electroplating electrolyte and other metal electroplating electrolytes. Quantum chemical calculations were employed to study the electronic properties and orbital information of the investigated complexing agents. The adsorption interactions between these complexing agents and the metal surfaces were investigated by molecular dynamic (MD) simulations. Consequently, the results of DFT calculations and MD simulations revealed that due to its strong electron donating abilities and high adsorption energies on metal surfaces, DMH could be the optimal choice from hydantoin derivatives as the complexing agent of the introduced cyanide-free gold electroplating electrolyte. This efficient and versatile method to study the mechanism of complexing agents' selection thus opens a new window to get insight views of coordination interaction and adsorption behaviour of complexing agents for metal ions and metal surfaces, respectively, during metal electroplating and will vigorously promote the level of this research region.

## **Acknowledgements**

Financial support from the State Key Laboratory of Urban Water Resource and Environment (Harbin Institute of Technology) (2015DX09) for this work is gratefully acknowledged.

## **References**

1. J. W. Ko, H. C. Koo, D. W. Kim, S. M. Seo, T. J. Kang, Y. Kwon, J. L. Yoon, J.

- H. Cheon, Y. H. Kim, J. J. Kim and Y. J. Park, *J. Electrochem. Soc.*, 2010, **157**, D46-D49.
2. A. He, Q. Liu and D. G. Ivey, *J. Mater. Sci. - Mater. Electron.*, 2009, **20**, 543-550.
3. Z. Liu and A. C. West, *Electrochim. Acta*, 2011, **56**, 3328-3333.
4. A. I. de Sa, S. Eugenio, S. Quaresma, C. M. Rangel and R. Vilar, *Thin Solid Films*, 2011, **519**, 6278-6283.
5. M. A. Barakat, Y. T. Chen and C. P. Huang, *App. Catal. B: Environ.*, 2004, **53**, 13-20.
6. M. Larsen, A. S. Ucisik and S. Trapp, *Environ. Sci. Technol.*, 2005, **39**, 2135-2142.
7. J. Doménech and J. Peral, *Solar Energy*, 1988, **41**, 55-59.
8. T. A. Green and S. Roy, *J. Electrochem. Soc.*, 2006, **153**, C157-C163.
9. J. S. Chen, Y. M. Fang, Q. Y. Qiu, L. X. You, J. Song, G. M. Zhang, G. N. Chen and J. J. Sun, *Green Chem.*, 2011, **13**, 2339-2343.
10. H. Honma and Y. Kagaya, *J. Electrochem. Soc.*, 1993, **140**, L135-L137.
11. X. Wang, N. Issaev and J. G. Osteryoung, *J. Electrochem. Soc.*, 1998, **145**, 974-981.
12. H. Watanabe, S. Hayashi and H. Honma, *J. Electrochem. Soc.*, 1999, **146**, 574-579.
13. S. Dimitrijevic, M. Rajcic-Vujasinovic and V. Trujic, *Int. J. Electrochem. Sci.*, 2013, **8**, 6620-6646.

14. M. Meusel and M. Gütschow, *Org. Prep. Proced. Int.*, 2004, **36**, 391-443.
15. G. Z. Pavlovich and R. G. Luthy, *Water Res.*, 1988, **22**, 327-336.
16. M. Puszyńska-Tuszkano, T. Grabowski, M. Daszkiewicz, J. Wietrzyk, B. Filip, G. Maciejewska and M. Cieślak-Golonka, *J. Inorg. Biochem.*, 2011, **105**, 17-22.
17. A. Liu, X. Ren, M. An, J. Zhang, P. Yang, B. Wang, Y. Zhu and C. Wang, *Sci. Rep.*, 2014, **4**, 3837.
18. A. Liu, X. Ren, B. Wang, J. Zhang, P. Yang, J. Zhang and M. An, *RSC Adv.*, 2014, **4**, 40930-40940.
19. A. Liu, X. Ren, J. Zhang, G. Yuan, P. Yang, J. Zhang and M. An, *New J. Chem.*, 2015, **39**, 2409-2412.
20. J. Zhang, A. Liu, X. Ren, J. Zhang, P. Yang and M. An, *RSC Adv.*, 2014, **4**, 38012-38026.
21. M. K. Nazeeruddin, F. De Angelis, S. Fantacci, A. Selloni, G. Viscardi, P. Liska, S. Ito, B. Takeru and M. Grätzel, *J. Am. Chem. Soc.*, 2005, **127**, 16835-16847.
22. H. Li, Y. Li and M. Chen, *RSC Adv.*, 2013, **3**, 12133-12139.
23. D. V. Deubel and T. Ziegler, *Organometallics*, 2002, **21**, 1603-1611.
24. S. Liang and A. E. Roitberg, *J. Chem. Theory Comput.*, 2013, **9**, 4470-4480.
25. W. Plazinski and M. Drach, *Appl. Surf. Sci.*, 2012, **262**, 153-155.
26. F. Rico, L. Gonzalez, I. Casuso, M. Puig-Vidal and S. Scheuring, *Science*, 2013, **342**, 741-743.

27. S. J. Zhou, D. L. Preston, P. S. Lomdahl and D. M. Beazley, *Science*, 1998, **279**, 1525-1527.
28. B. Saha, S. Shindo, S. Irle and K. Morokuma, *Acs Nano*, 2009, **3**, 2241-2257.
29. K. Honkala, A. Hellman, I. N. Remediakis, A. Logadottir, A. Carlsson, S. Dahl, C. H. Christensen and J. K. Norskov, *Science*, 2005, **307**, 555-558.
30. M. Altarawneh, M. W. Radny, P. V. Smith, J. C. Mackie, E. M. Kennedy and B. Z. Dlugogorski, *Appl. Surf. Sci.*, 2008, **254**, 4218-4224.
31. M. E. Tuckerman, D. Marx, M. L. Klein and M. Parrinello, *Science*, 1997, **275**, 817-820.
32. G. Agalya, C. Lv, X. Wang, M. Koyama, M. Kubo and A. Miyamoto, *Appl. Surf. Sci.*, 2005, **244**, 195-198.
33. B.-Y. Tang, M.-D. Chen, K.-L. Han and J. Z. H. Zhang, *J. Phys. Chem. A*, 2001, **105**, 8629-8634.
34. R. Chen, M. Liang, J. Luo, H. Lei, D. Guo and X. Hu, *Appl. Surf. Sci.*, 2011, **258**, 1756-1761.
35. H. Chermette, *Coord. Chem. Rev.*, 1998, **178-180**, 699-721.
36. G. Harrach, Z. Valicsek and O. Horváth, *Inorg. Chem. Commun.*, 2011, **14**, 1756-1761.
37. C. I. Maxwell, A. A. Neverov, N. J. Mosey and R. Stan Brown, *J. Phys. Org. Chem.*, 2014, **27**, 419-429.
38. H.-T. Liu, X.-G. Xiong, P. D. Dau, Y.-L. Wang, J. Li and L.-S. Wang, *Chem. Sci.*, 2011, **2**, 2101-2108.

39. S. L. Daifuku, M. H. Al-Afyouni, B. E. R. Snyder, J. L. Kneebone and M. L. Neidig, *J. Am. Chem. Soc.*, 2014, **136**, 9132-9143.
40. D. R. Armstrong, S. E. Baillie, V. L. Blair, N. G. Chabloz, J. Diez, J. Garcia-Alvarez, A. R. Kennedy, S. D. Robertson and E. Hevia, *Chem. Sci.*, 2013, **4**, 4259-4266.
41. T. Wang, Y. Liang and Z. X. Yu, *J. Am. Chem. Soc.*, 2011, **133**, 9343-9353.
42. C. Wang, M. An, P. Yang and J. Zhang, *Electrochem. Commun.*, 2012, **18**, 104-107.
43. C. Wang, J. Zhang, P. Yang and M. An, *Electrochim. Acta*, 2013, **92**, 356-364.
44. A. Kokalj, S. Peljhan, M. Finšgar and I. Milošev, *J. Am. Chem. Soc.*, 2010, **132**, 16657-16668.
45. J. Zhang, G. Qiao, S. Hu, Y. Yan, Z. Ren and L. Yu, *Corros. Sci.*, 2011, **53**, 147-152.
46. R. Hasanov, M. Sadıkoğlu and S. Bilgiç, *Appl. Surf. Sci.*, 2007, **253**, 3913-3921.
47. S. Xia, M. Qiu, L. Yu, F. Liu and H. Zhao, *Corros. Sci.*, 2008, **50**, 2021-2029.
48. R. M. Issa, M. K. Awad and F. M. Atlam, *Appl. Surf. Sci.*, 2008, **255**, 2433-2441.
49. A. Liu, X. Ren, J. Zhang, C. Wang, P. Yang, J. Zhang, M. An, D. Higgins, Q. Li and G. Wu, *RSC Adv.*, 2014, **4**, 40606-40616.
50. N. Kovačević and A. Kokalj, *J. Phys. Chem. C*, 2011, **115**, 24189-24197.
51. S. Issaadi, T. Douadi and S. Chafaa, *Appl. Surf. Sci.*, 2014, **316**, 582-589.

52. Z. Rinkevicius, X. Li, J. A. R. Sandberg, K. V. Mikkelsen and H. Ågren, *J. Chem. Theory Comput.*, 2014, **10**, 989-1003.
53. W. T. Cahyanto, G. Shukri, M. K. Agusta and H. Kasai, *Appl. Surf. Sci.*, 2013, **266**, 405-409.
54. A. Kokalj, P. Gava, S. de Gironcoli and S. Baroni, *J. Phys. Chem. C*, 2008, **112**, 1019-1027.
55. N. K. Das and T. Shoji, *Appl. Surf. Sci.*, 2011, **258**, 442-447.
56. F. Y. Guo, C. G. Long, J. Zhang, Z. Zhang, C. H. Liu and K. Yu, *Appl. Surf. Sci.*, 2015, **324**, 584-589.
57. S. Peljhan and A. Kokalj, *J. Phys. Chem. C*, 2009, **113**, 14363-14376.
58. M. Zhang, K. Yang and Y. Yu, *Appl. Surf. Sci.*, 2015, **328**, 583-590.
59. X. Ren, Y. Song, A. Liu, J. Zhang, P. Yang, J. Zhang, G. Yuan, M. An, H. Osgood and G. Wu, *RSC Adv.*, 2015, **Manuscript ID: RA-ART-06-2015-012217 (under revision)**.
60. S. El Issami, L. Bazzi, M. Mihit, B. Hammouti, S. Kertit, E. A. Addi and R. Salghi, *Pigm. Resin. Technol.*, 2007, **36**, 161-168.
61. K. Barouni, L. Bazzi, R. Salghi, M. Mihit, B. Hammouti, A. Albourine and S. El Issami, *Mater. Lett.*, 2008, **62**, 3325-3327.

**Figure captions:**

**Fig. 1** Macroscopic images of gold electrodeposits obtained from the introduced cyanide-free gold electroplating electrolyte, (a) with additive, (b) without additive, and (c) from H<sub>AuCl</sub><sub>4</sub> electrolyte without DMH.

**Fig. 2** SEM images of the top views of gold electrodeposits obtained from the introduced cyanide-free gold electroplating electrolyte, (a) and (b) with additive, (c) and (d) without additive, as well as (e) and (f) from H<sub>AuCl</sub><sub>4</sub> electrolyte without DMH.

**Fig. 3** The XRD patterns of (a) Au (JCPDS file: 04-0784) and gold electrodeposits obtained from the introduced cyanide-free gold electroplating electrolyte, (b) with additive, (c) without additive, and (d) from H<sub>AuCl</sub><sub>4</sub> electrolyte without DMH.

**Fig. 4** Schematic diagrams of frontier molecular orbitals of (a) AHD, (b) BCDMH, (c) DBDMH, (d) DCDMH, (e) DMDMH, (f) DMH, (g) Hydantoin, (h) TMH.

**Fig. 5** Charge distributions of (a) AHD, (b) BCDMH, (c) DBDMH, (d) DCDMH, (e) DMDMH, (f) DMH, (g) Hydantoin, (h) TMH (unit of e).

**Fig. 6** Adsorption behaviors of AHD on the Au surface, (a) Initial configuration of the simulation box (AHD visualized by balls and sticks, water molecule visualized by lines). (b) Final equilibrium configuration of the MD simulation box (c) Top view of the final equilibrium configuration of the simulation box. (d) Energy fluctuation curves of the MD simulation. (e) Temperature fluctuation curve of the MD simulation.

**Figures:**

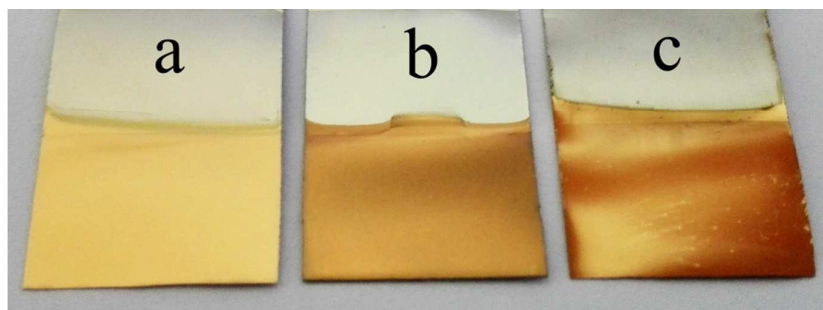


**Fig. 1** Macroscopic images of gold electrodeposits obtained from the introduced cyanide-free gold electroplating electrolyte, (a) with additive, (b) without additive, and (c) from  $\text{HAuCl}_4$  electrolyte without DMH.

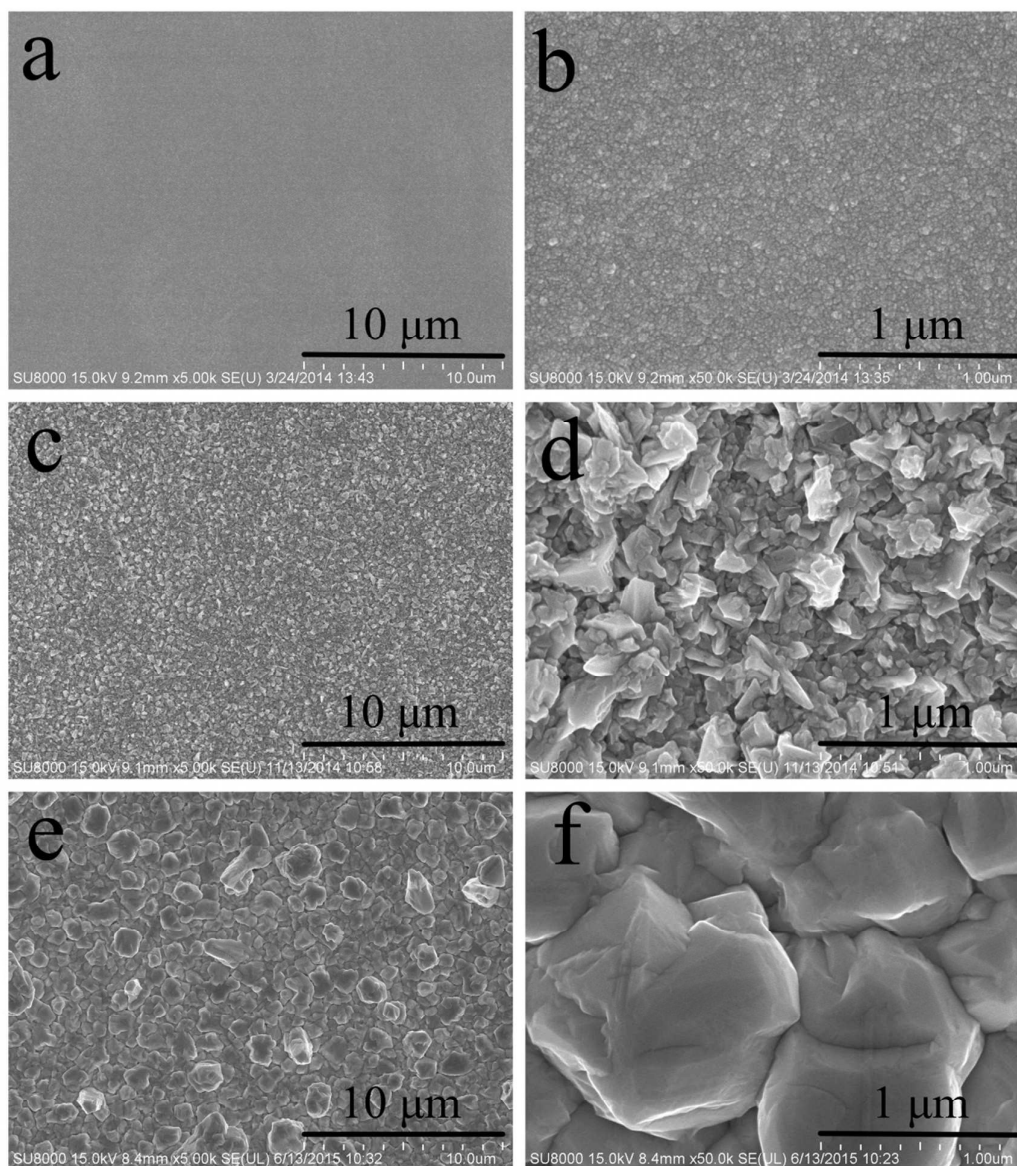


**Fig. 2** SEM images of the top views of gold electrodeposits obtained from the introduced cyanide-free gold electroplating electrolyte, (a) and (b) with additive, (c) and (d) without additive, as well as (e) and (f) from  $\text{HAuCl}_4$  electrolyte without DMH.

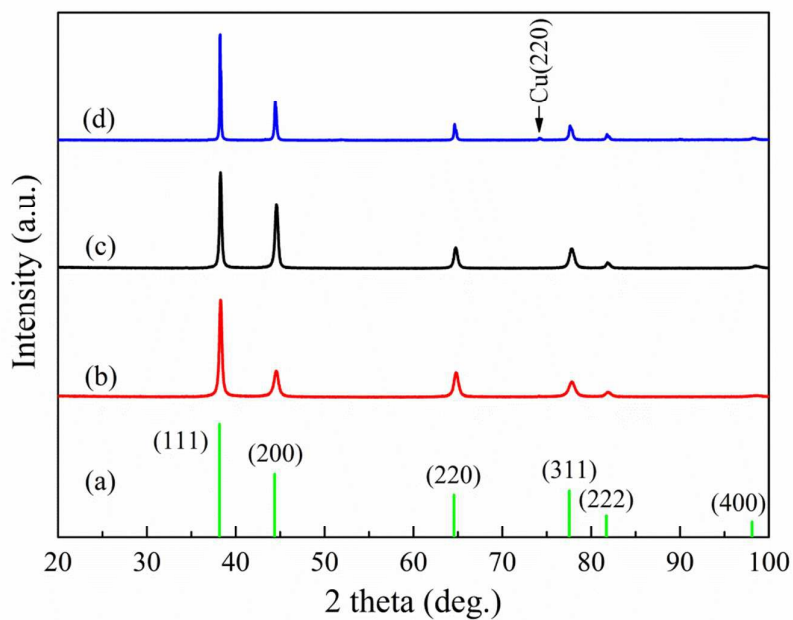


**Fig. 3** The XRD patterns of (a) Au (JCPDS file: 04-0784) and gold electrodeposits obtained from the introduced cyanide-free gold electroplating electrolyte, (b) with additive, (c) without additive, and (d) from H<sub>2</sub>AuCl<sub>4</sub> electrolyte without DMH.

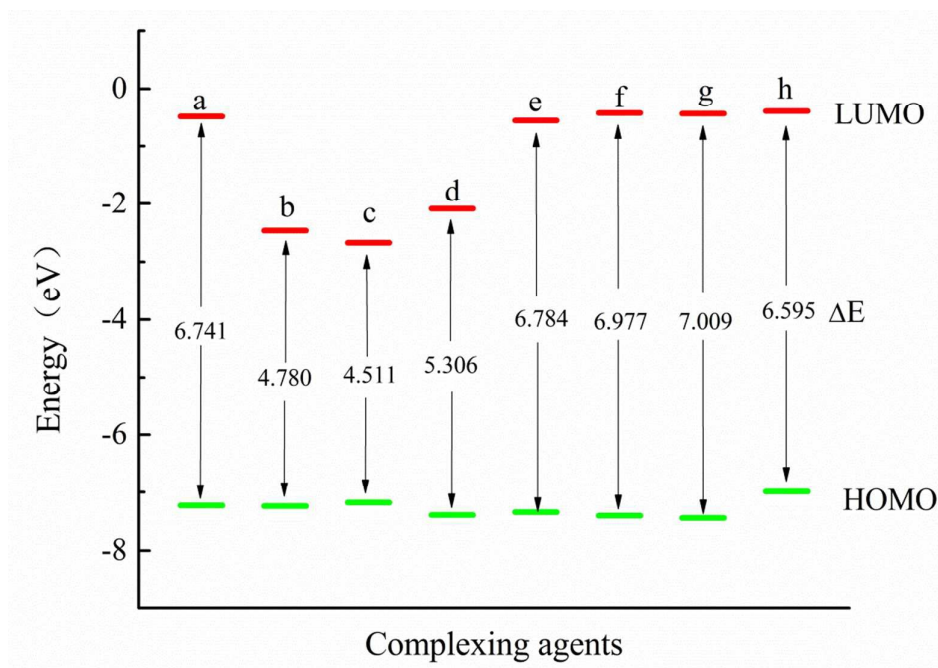


**Fig. 4** Schematic diagrams of frontier molecular orbitals of (a) AHD, (b) BCDMH, (c) DBDMH, (d) DCDMH, (e) DMDMH, (f) DMH, (g) Hydantoin, (h) TMH.

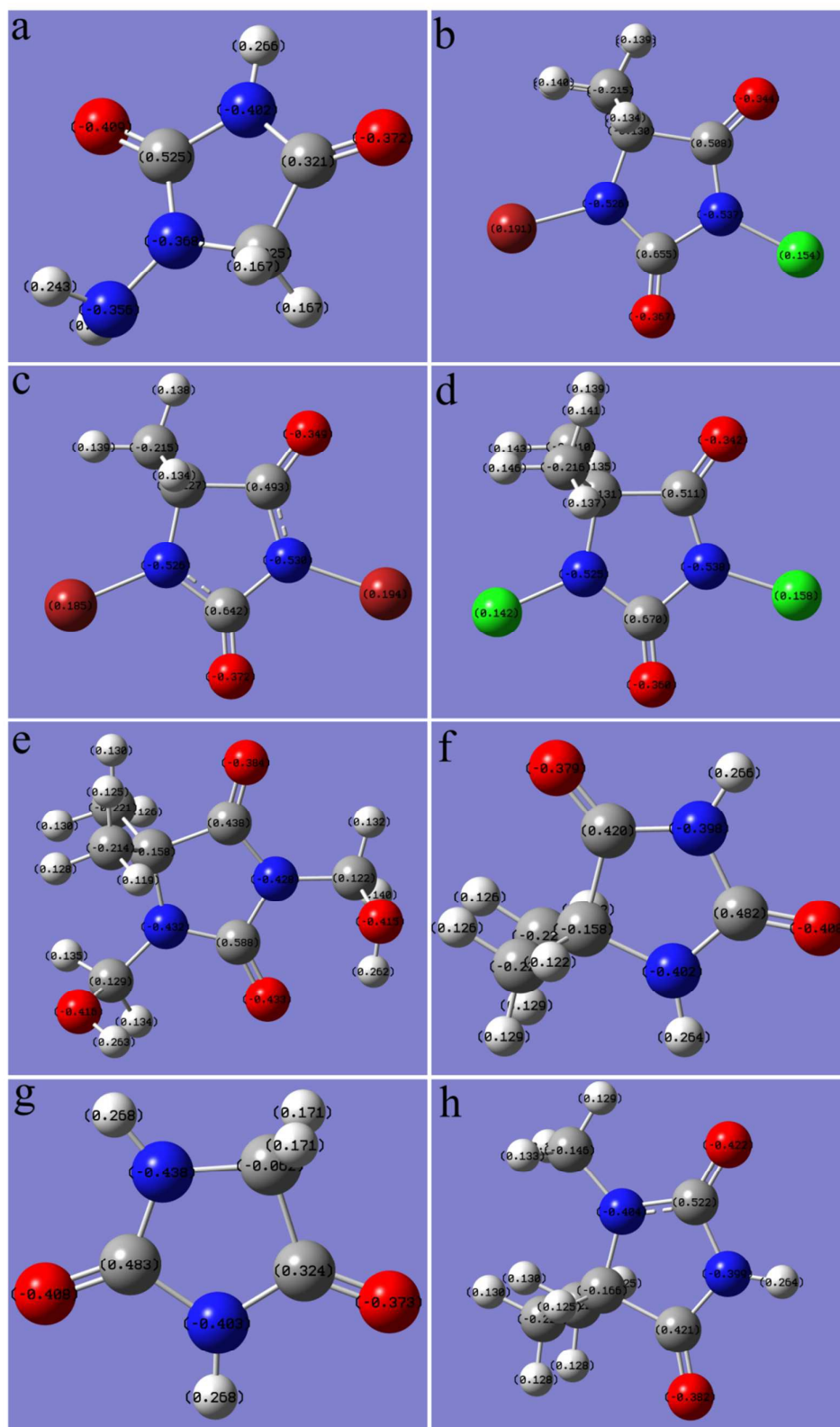


**Fig. 5** Charge distributions of (a) AHD, (b) BCDMH, (c) DBDMH, (d) DCDMH, (e) DMDMH, (f)

DMH, (g) Hydantoin, (h) TMH (unit of e).

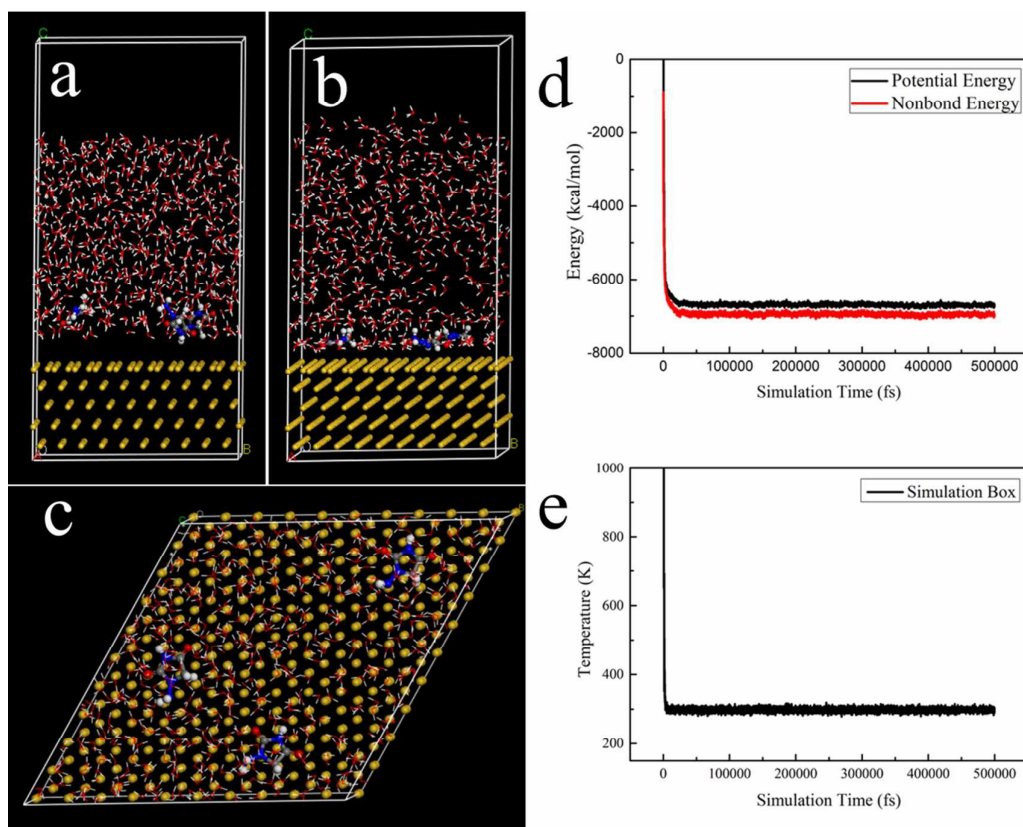


**Fig. 6** Adsorption behaviors of AHD on the Au surface, (a) Initial configuration of the simulation box (AHD visualized by balls and sticks, water molecule visualized by lines). (b) Final equilibrium configuration of the MD simulation box (c) Top view of the final equilibrium configuration of the simulation box. (d) Energy fluctuation curves of the MD simulation. (e) Temperature fluctuation curve of the MD simulation.

**Table:****Table 1** Adsorption energies of all the studied complexing agents on Ni (111) and Au (111) surface.

(unit of kJ/mol)

		Ni(111)	Au(111)
a	Aminohydantoin (AHD)	244.760	314.881
b	BCDMH	244.312	337.349
c	DBDMH	290.857	288.399
d	DCDMH	201.312	266.578
e	DMDMH	297.777	305.429
f	DMH	248.861	289.469
g	Hydantoin	259.131	217.384
h	TMH	298.177	339.674